Research Article Vol. 5, No. 2 / 15 Feb 2026 / Optics Continuum 651
OPTICS CONTINUUM

Analytic results for the partially coherent edge response of a perfect imaging system

JOSEPH J. M. BRAAT*

Department of Imaging Physics, Delft University of Technology, Delft, The Netherlands
*joseph.braat@gmail.com

Abstract: The edge response of a perfect optical system with partially coherent object illumination is characterized, among other things, by its central intensity in the image plane, that is, the intensity in the image plane at the position of an infinitely sharp knife-edge transition as predicted by the geometrical optics approximation. Other important parameters are the central steepness and the typical oscillations of the edge response in the image plane. I produce a new analytic expression for the value of the central intensity in a one-dimensional optical system as a function of the degree of coherence in the illuminated object. This new result is then successfully implemented by me in the more common two-dimensional imaging systems. To obtain the full intensity profile of the edge response, I switch to Fourier imaging analysis by periodic continuation of the knife-edge object. A comparison is made between the exact value of the central intensity obtained in the spatial domain and the corresponding (approximated) values resulting from the Fourier domain analysis. The edge response of an optical imaging system plays an important role in optical precision metrology. In my analysis, I evaluate the systematic errors (aliasing) that are associated with intensity calculations in the Fourier domain as a function of the frequency sampling density.

1. Introduction

To obtain the (diffraction) image of a coherently illuminated planar object by an optical system, one generally carries out a convolution of the spatially varying complex transmission function of the object and the complex amplitude impulse response function of the optical imaging system. For an ideal and perfectly focused optical system with circular symmetry, the impulse response equals the amplitude of the Airy diffraction pattern associated with a circular pupil. Such a convolution integral needs to be executed for each individual image point. For an incoherent imaging of the object by the same ideal optical system, one uses the intensity transmission function of the planar object and convolves it with the intensity version of the Airy diffraction pattern. Such a simple change in the imaging formalism is not possible when the object is illuminated by a partially coherent beam and the coherence region in the object plane has neither a vanishing small extent (incoherent illumination) nor a very large size (coherent illumination). I will cover the subject of partially coherent illumination of the object plane in section 2 for spatial domain calculations and in section 3 for calculations in the Fourier domain.

Fourier-based analysis of the optical imaging process uses the spatial spectral content of the object transmission function and considers the imaging system as a spatial frequency filter. Both for the coherent and the incoherent case, the resulting spatial frequency function associated with the optical image is the *product* of the object frequency function and the imaging filter function associated with an ideal optical system. The imaging filter function is commonly called the optical transfer function (*OTF*) of the optical system. For coherent imaging the *OTF* is given by the scaled pupil function of the lens itself, for incoherent imaging the *OTF* is given by the normalized autocorrelation function of the lens pupil function. The image frequency spectrum is

#575658 https://doi.org/10.1364/OPTCON.575658
Journal © 2026 Received 8 Aug 2025; revised 19 Jan 2026; accepted 19 Jan 2026; published 2 Feb 2026

OPTICS CONTINUUM

again given by a simple product of the object spectrum function and the *OTF* of the imaging system. When comparing the two approaches, one observes the following calculation steps:

- *Spatial domain* (N^2 image points, two-dimensional object / image)
  - Calculation (N^2 times) of the 2D convolution integral of the object function and the impulse response.
  - The integer N is determined by the impulse response. The distance between two subsequent points in the image plane should be chosen equal to or smaller than typically 1/4 of the diffraction unit in the image plane.
  - In the particular case of a one-dimensional object structure, such as a knife-edge object, N^2 reduces to N.
  - Practical values of N for an extended image could be as large as 1000.
- *Fourier domain* (two-dimensional object / image)
  - Calculation of a 2D (fast) Fourier transform (*FFT*) of the object function, yielding $\mathcal{F}_o$
  - Multiplication of $\mathcal{F}_o$ with the analytically available *OTF* function yields the Fourier transform of the image plane function, $\mathcal{F}_i$
  - inverse 2D *FFT* of $\mathcal{F}_i$ to obtain the required image function in the spatial domain.

As we stated above, the two procedures apply to linear imaging as encountered in fully coherent or fully incoherent imaging systems.

Inspection of the two approaches suggests that, with respect to numerical calculation effort, the Fourier domain approach is advantageous as compared to the spatial domain calculations with its tedious convolution integrals containing the oscillating impulse response function. Another advantage of the Fourier approach is the strict separation of the transformed object function $\mathcal{F}_0$ and the frequency transfer function *OTF* of the optical system. The latter has to be calculated a single time, then stored and can be repeatedly used in the multiplication process of *OTF* and $\mathcal{F}_0$ if multiple object functions need to be processed.

A further simplification of the Fourier domain calculations is obtained if the object function is periodic. The Fourier transform $\mathcal{F}_0$ is then replaced by a Fourier series with a finite number of terms. Even if an object is non-periodic, such as a knife-edge, it can be made quasi-periodic by periodic continuation. For the 1D knife-edge object, the object function is first given a finite extent by multiplying it with a (centered) rectangular function of width d. This object of width d is then repeated periodically with its center at distances $x = \pm nd$ for integer values of n, yielding a 1D periodic function. Unfortunately, in practice, the Fourier series which yields the desired edge response has to be truncated for obvious practical reasons (storage space, calculation time). Therefore, the Fourier-based edge response intensity will suffer from residual errors like aliasing.

In this paper I limit myself to a scalar treatment of the optical diffraction effects. If needed, specific states of electromagnetic polarization, perpendicular or parallel to the knife-edge object, can be individually treated. Scalar treatment of two perpendicular polarization components yields reliable results for moderate values of the lens apertures, up to 0.5, and they can be combined again in the low aperture section of an imaging system. Beyond such an aperture value, numerical simulation of the electromagnetic diffraction effects is needed to include effects that are missed by the scalar diffraction approach.

1.1. Derivation of the edge response in the spatial domain

The image of a flat object can be obtained with the aid of elementary response functions. As examples of such response functions, one can mention the point-spread function, the line-spread function, and the edge response function (for a one-dimensional (1D) object structure). In the

OPTICS CONTINUUM

latter case, the image of a (knife) edge in the object plane is considered with an infinitely sharp transition in transparency or reflectivity from zero to one (the so-called 'absorbing half-plane'). In the case of an edge object, the edge response can be simply obtained from a 1D optical system with cylindrical optics and 1D illumination optics with a line-shaped source of infinitely small or finite width.

In practice, each response function has two extreme versions. As mentioned before, there are the complex amplitude and the intensity version. The image plane amplitude/intensity are then calculated by means of a convolution of the corresponding versions of the transmission function of the object and the impulse response function of the optical system. Full spatial coherence in the object plane is present when the illuminating source is point-like, at a finite or infinitely large distance; in the latter case, we have plane wave illumination with a solid angle extent approaching zero. Complete incoherence in the spatial domain is obtained when an extended source illuminates the object plane from all directions within a solid angle of 2π. In this paper the two extreme cases of zero and 2π solid angle illumination are considered *and* all values in between, the so-called region of partially coherent object illumination.

The edge response is evaluated in the image plane of a conventional imaging system; as an example a microscope is chosen, with its illumination (condenser) part and imaging section (both 1D- and 2D imaging systems will be considered). As mentioned in the abstract, I will first focus on the normalized central intensity in the image plane of a conventional imaging system. In Fig. 1(a) we have depicted such a conventional system with the knife edge at the point C_o in the center of the object plane O_1; the knife-edge itself has the coordinate $y_n = 0$. The intensity measured at the center C_i of the image plane with coordinate $y'_n = 0$ will be denoted by $I_c(0)$, the normalized *central* intensity. For the value of $I_c(0)$, see the red dot on the accompanying drawing of a possible image intensity profile $I(y'_n)$ in the plane at $z'_n = 0$.

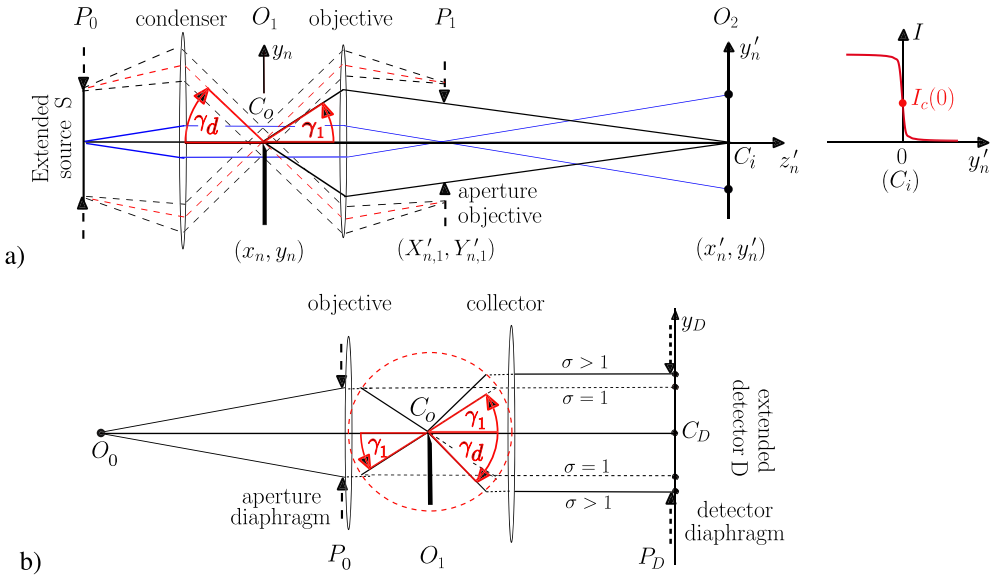

Fig. 1. a) A conventional imaging system, with an illumination (condenser) and imaging (objective) section. b) Auxiliary measurement scheme according to Zernike. This scheme enables the comprehensible calculation of the central intensity $I_c(0)$ that is found at the point C_i in the image plane O_2 of the conventional imaging system in a).

In the limit of incoherent object illumination, it is well known that $I_c(0)$ equals 0.5 after normalization with the central intensity value (equal to unity) in the absence of an object (see

OPTICS CONTINUUM

Fig. 1, when summing all the forward-diffracted light intensity after the knife-edge that reaches the image point C_i). When using the edge response of an optical system for optical metrology (e.g. in optical lithography) it would be preferable that the geometrical position of the knife-edge coincides with the measured 50% level of the detected intensity profile in the image plane of a conventional imaging system. However, depending on the partial coherence of the knife edge illumination in the imaging system, the value of $I_c(0)$ will be smaller than 50%. For instance, for coherent illumination, half of the complex amplitude is transmitted by the edge object, and, after squaring the accumulated complex amplitude of 0.5 in the very center of the image plane at C_i, a normalized intensity value $I_c(0) = 0.25$ is measured. The value of $I_c(0)$ for general illumination conditions should be calculated with high precision to avoid metrological errors. When combining two edge objects to obtain an absorbing or transmitting slit, one also needs to calculate not only the value of $I_c(0)$ but also the full shape of the edge response function under general illumination conditions of the edge object.

In Fig. 1(b) we show an elegant method to calculate $I_c(0)$ for the general case of partially coherent illumination of an isolated edge object e.g. in a conventional microscope. It has been put forward by Zernike as an auxiliary system in his well-known publication from 1934 [1] (translated in 2002 from the German to the English language in [2]). It has been demonstrated by Zernike that the desired value of $I_c(0)$ in a conventional imaging system according to Fig. 1(a) is given by the normalized integrated intensity, measured by the far-field detector D in Fig. 1(b). The influence on $I_c(0)$ of the partial coherence in the conventional imaging system is simply taken care of by a proper adjustment of the diaphragm P_D in front of the detector D with its center at C_D in Fig. 1(b).

In Zernike's auxiliary system of Fig. 1(b) a spherical wave is emitted by the source point at O_0 and is focused in the plane O_1 at the point C_o by a perfect objective with an aperture value of $\sin\gamma_1$. The wave diffracted by the knife-edge at C_o is captured by the collector lens and projected on the extended detector D. The collector lens preferably satisfies the Abbe sine condition. This means that the sine of a general ray angle γ_d in the object space of the collector lens and the intersection point with coordinate y_D of the ray with the detector surface D have the linear relationship $y_D = f_c \sin\gamma_d$ (f_c is the image-side focal distance of the collector lens). The collecting area of the detector D is determined by the sine of the maximum acceptance angle, $\sin\gamma_d$, which, in turn, is determined by the lateral size of the detector diaphragm P_D.

In a conventional microscope a partial 'incoherence' factor σ in the object plane is defined by the ratio of the condenser aperture and the objective aperture. In an analogous way, the partial incoherence factor σ in Zernike's detection scheme is given by the 'incoherence' ratio

$$\sigma = \frac{\sin\gamma_d}{\sin\gamma_1}. \tag{1}$$

The detection scheme used by Zernike has been formalized by Welford [3] who showed that the integrated intensity according to Zernike can be made identical to the normalized on-axis intensity in a conventional microscope, by exchanging the roles of the microscope condenser lens and the collector lens in Zernike's set-up when carrying out the calculations. The point-by-point intensity response of a general 2D-object can be obtained in Zernike's scheme by a lateral line scan of the object in the object plane O_1, followed by subsequent perpendicular displacements. Such a scanning system (called a *flying-spot* scanner) was first reported by Minsky [4]. Welford [5] introduced the term scanning microscopy, as opposed to conventional microscopic imaging (for this subject, see also [6,7]). The detection optics in an optical disc player for e.g. CD, DVD, Blu Ray [8,9,10] are also based on Zernike's detection scheme, with the incoherence factor σ generally equal to 1.

OPTICS CONTINUUM

1.2. Overview of the paper

In section 2, by means of calculations in the spatial domain, I derive an exact expression for the central intensity $I_c(0)$ of the edge response for a 1D optical system having an arbitrary value of the incoherence factor σ. I apply this result to the corresponding 2D imaging system, where I obtain arbitrarily accurate results with a known residual error. In section 3 I calculate the complete edge response function by calculations in the discrete Fourier domain, using the periodic continuation of a finite part with width d of the knife-edge object function. The advantage of this approach is the simple and fast calculation of off-axis values of the spatial edge response by multiplication of the calculated Fourier series data with simple complex exponential functions of position and spatial frequency. In section 4 I study the accuracy of the Fourier results for the edge response as a function of the period d used in the periodic continuation process. I also use exact values for the cross-correlation coefficients that are needed in the Fourier calculations. For an ideal optical system, these coefficients are given by the area of overlap of three mutually offset circles; the size of their common area has been analytically evaluated by me. I then exploit the fact that, for comparison, I have at my disposal the exact values of the 1D spatial edge response and very accurate results with known residual error for the 2D spatial edge response. The deviations between the spatial domain and the Fourier results are thus only due to deviations (discrete sampling and truncation) associated with imperfect Fourier modeling. Finally, in section 5, I present the conclusions about these parallel calculations in the spatial domain and in the Fourier domain with respect to the resulting edge response. And I establish the relation between the value of the periodic continuation distance d (expressed in the diffraction unit $\lambda/\sin\gamma_1$ corresponding to the imaging objective) and the residual error in the Fourier results due to aliasing effects.

2. Spatial domain calculation of the central intensity $I_c(0)$ in a knife-edge image

In Fig. 2 Zernike's auxiliary scheme is reproduced for the calculation of $I_c(0)$ in a 1D (or 2D) optical system. Due attention is paid to the various (normalized) coordinate systems in the apertures P_0 and P_1 and in the the object plane O_1 and the detector plane at D. The aperture and detector coordinates, (X_n, Y_n) and (p, q), have been normalized with respect to the lateral radius ρ_{P_0} of the objective aperture. The coordinates (x_n, y_n) in the plane O_1 have been normalized with respect to the diffraction unit $\lambda/\sin\gamma_1$ in the object plane O_1 (λ is the wavelength of the light in the medium). Likewise, spatial frequencies (u_x, u_y) will be normalized with respect to the quantity $\sin\gamma_1/\lambda$, yielding a normalized frequency pair $(u_{x,n}, u_{y,n})$. For the aberration-free imaging case, Zernike identifies the intensity pattern on the surface Σ_1 within the collecting area P_1 as a constant plus a Legendre function of the second kind of order zero, $Q_0(Y_{n,1})$. Outside the unit pupil area P_1 the intensity value is exclusively determined by the Legendre function $Q_0(Y_{n,1})$.

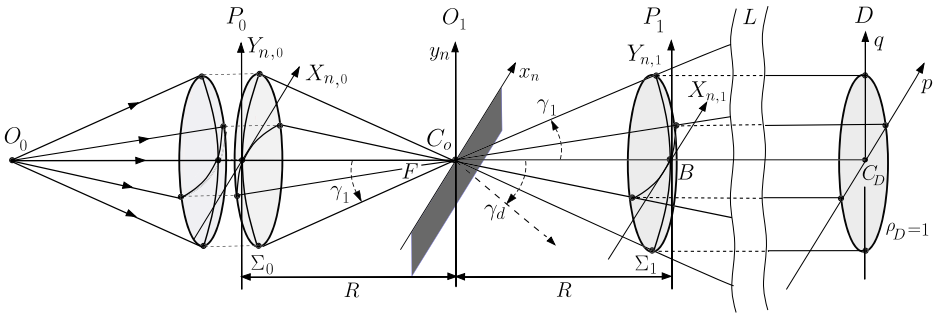

Fig. 2. The same legend for a Zernike auxiliary scheme as in Fig. 1(b), now for an elaborated 2D version.

OPTICS CONTINUUM

In Fig. 2, after the collecting aperture P_1, a lens system L has been added to project the optical field, diffracted by the knife edge, on the light collecting detector surface D. As it was mentioned before, the lens L should satisfy Abbe's sine condition. In Fig. 2 the special case is shown of equality in lateral size of the aperture P_0 of the focusing optics, of the collecting aperture at P_1 and the planar surface D with a normalized radius ρ_D equal to one). Of course, other cases with arbitrary collecting areas can be accommodated in Zernike's auxiliary scheme, such that the normalized radius ρ_D assumes any value σ ranging from 0 to $1/\sin\gamma_1$. In the figure, this possibility is suggested by a general diffraction angle γ_d for diffracted light, which can still be accommodated by the optics if the lateral extent of the collecting aperture P_1 and the collecting area at D are properly adjusted.

Zernike discusses the influence of the imaging aperture $\sin\gamma_1$ at C_o and the light collecting aperture P_1 on the normalized *integrated* intensity on the detector D in Fig. 2, which finally yields the value of $I_c(0)$ in the conventional image of a knife edge. He first presents the values of $1/2$ ($\sigma \to \infty$) and $1/4$ ($\sigma \to 0$). Almost in passing, by means of footnote 1 on page 698 of Ref. [1], he then mentions a third value of $1/3$ which should follow from the values of two integrals that are needed to arrive at this analytic value of $1/3$ for $I_c(0)$. This specific value corresponds to the frequently occurring case of equal objective and collector apertures (incoherence factor $\sigma = 1$, $\rho_D = 1$).

2.1. Calculation of the far-field intensity of a knife-edge object

In Zernike's scheme, the light diffracted by the (centered) knife-edge propagates towards a reference surface Σ_1 through the point B, see Fig. 2. The coordinates on this reference surface are equal to the normalized coordinates on the wavefront Σ_0, provided with the modified index 1, viz. $(X_{n,1}, Y_{n,1})$. In the absence of the knife-edge, the light flux will be (sharply) limited to the gray-shaded region of the surface Σ_1, especially when a field lens would be present in the focal plane through F. With the knife-edge in place, there will be an appreciable amount of light diffracted in the vertical $Y_{n,1}$-direction. Using a schematically drawn lens L with focal distance $f = R$, that satisfies the Abbe sine condition, the intensity distribution is projected from the curved surface Σ_1 onto the planar detector surface D, with its center in C_D. As a result, the coordinates (p, q) of a ray incident on the detector D are equal to the coordinates $(X_{n,1}, Y_{n,1})$ of the intersection point of the same ray with the surface Σ_1. The signal detected by the extended detector D yields the edge response when the knife-edge is scanned along the y_n-axis. The requested signal value $I_c(0)$ is obtained when the knife-edge is positioned exactly at $y_n = 0$. For such a well-centered knife-edge, the value of $I_c(0)$ provides us, for instance, with information on the σ-value in the auxiliary set-up. In Fig. 2 a diffracted ray at an angle γ_d with the optical axis has been schematically shown; such ray directions give rise to a circular disk with the normalized radius $\sigma = \sin\gamma_d/\sin\gamma_1$ on the detector D.

2.2. Far-field intensity distribution of a knife-edge object illuminated by a focused beam

2.2.1. 1D-geometry (spatial domain)

The object transmission function $t(x_n, y_n)$ of a knife-edge object according to Fig. 2 is given by,

$$t(x_n, y_n) = H(y_n) = \tfrac{1}{2}\{1 + \mathrm{sgn}(y_n)\} = \begin{cases} 0, & y_n<0, \\ \frac{1}{2}, & y_n = 0, \\ 1, & y_n>0\,. \end{cases} \tag{2}$$

$H(y_n)$ denotes the Heaviside function and $\mathrm{sgn}(y_n)$ is the signum-function.

OPTICS CONTINUUM

In his 1D analysis, Zernike gives the far-field complex amplitude $A(Y_{n,1})$ on the surface Σ_1 and $A(q)$ on the detector D,

$$A(q) = \frac{1}{2}\,\mathrm{rect}\left[\frac{q}{2}\right] + \frac{i}{2\pi}\,\ln\left(\frac{1+q}{1-q}\right), \qquad |q|<1. \tag{3a}$$

$$= \frac{i}{2\pi}\,\ln\left(\frac{q+1}{q-1}\right), \qquad |q|>1, \tag{3b}$$

where the rect-function with width 2 determines the lateral size of the non-diffracted part of the incident beam with an amplitude of $1/2$. For the 1D-case, the incoherence factor σ determines the height 2σ of the strip-detector through C_D that is effectively used for light intensity collection, see Fig. 2.

An amplitude singularity arises at $q = \pm 1$. In practice, a high intensity level is found at the images at P_1 of the two borders of the cylindrical optics at P_0. Mathematically, integration of the corresponding intensity, see Eq. (4), yields a finite value for the Cauchy principal value of the integral. The finite result for this intensity integral could be physically expected since the integrated intensity of the field that is incident on the knife-edge object is also finite (normalized to unity). Similar arguments hold for the singularities that are present in Eqs. (5) and (6). The intensity distribution on the detector follows immediately from Eq. (3) and is given by

$$I(q) = \frac{1}{4}\mathrm{rect}\left[\frac{q}{2}\right] + \frac{1}{4\pi^2}\,\ln^2\left(\frac{1+q}{1-q}\right), \qquad |q|<1, \tag{4a}$$

$$= \frac{1}{4\pi^2}\,\ln^2\left(\frac{q+1}{q-1}\right), \qquad |q|>1\,. \tag{4b}$$

2.2.2. 2D geometry (spatial domain)

The extension to two dimensions is straightforward, see [11,12,13]. The complex amplitude on the curved surface Σ_1 in Fig. 2 is the Fourier transform of the complex amplitude in the object plane O_1. This complex amplitude is the product of an Airy disk (the diffraction image at C_o, produced by the lens with pupil P_0) and the transmission function $t(x_n, y_n)$ of the knife-edge. The Fourier transform on the surface Σ_1 (and on the detector surface D) thus is the convolution of the pupil function P_0, equal to $\mathrm{circ}([p^2+q^2]^{1/2})$, and the Fourier transform of the Heaviside function $H(y_n)$ of Eq. (2). The resulting complex amplitude $A(p,q)$ on the surface of detector D is then given by

$$A(p,q) = \frac{1}{2}\mathrm{circ}\left(\sqrt{p^2+q^2}\right) + i\,\frac{1}{2\pi}\,\ln\left|\frac{\sqrt{1-p^2}+q}{\sqrt{1-p^2}-q}\right|, \qquad |p| \le 1\,. \tag{5}$$

The intensity distribution on the detector, as a function of the coordinates (p,q), is given by

$$I(p,q) = \frac{1}{4}\left\{\mathrm{circ}\left(\sqrt{p^2+q^2}\right) + \frac{1}{\pi^2}\,\ln^2\left|\frac{\sqrt{1-p^2}+q}{\sqrt{1-p^2}-q}\right|\right\}, \quad |p| \le 1\,. \tag{6}$$

The far-field intensity distributions $I(q)$ (1D) and $I(p,q)$ (2D) on the detector D have been depicted in Fig. 3. For a 1D system, the strip-like detection area has a height 2σ. For a 2D optical system with a circular objective pupil P_0, the circular detection region has a diameter 2σ. To increase the visibility of the intensity contours in Fig. 3, the darker features in b) and c) correspond to the more intense light levels. There is no absolute relationship between the contour levels in the plots b) and c).

For the 1D and 2D optical systems, the central intensity $I_c(0)$ produced by a knife-edge is obtained by integrating the light intensity in Fig. 3 over the detector area D with its typical size

OPTICS CONTINUUM

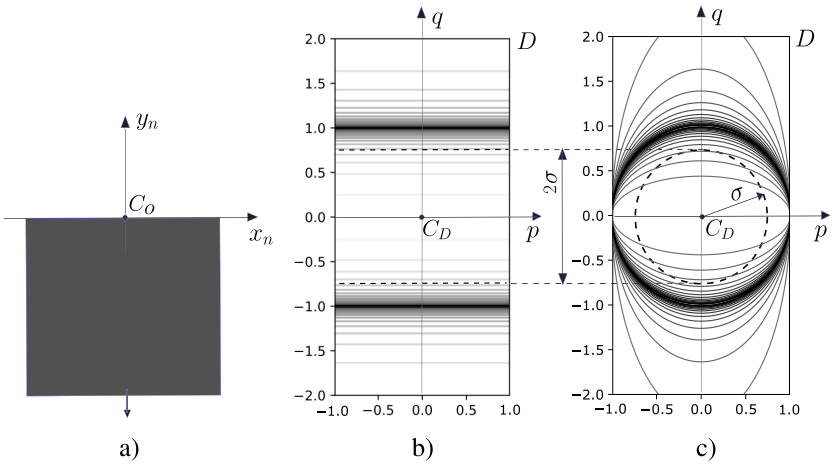

Fig. 3. a) Orientation of the knife-edge in the 'scanning' object plane through C_o. b) The far-field intensity distribution $I(q)$ in the detector plane D (center at C_D) for a 1D optical system with line-source illumination and a detection area with height 2σ. c) Same as for b) but now for a 2D optical system with intensity distribution $I(p, q)$; detection area is the disk with diameter 2σ (dashed in the figure).

of 2σ. In Fig. 2 both apertures have been taken equal ($\sigma = 1$), but, in practice, any σ-value in the range $0<\sigma<(1/\sin\gamma_1)$ is feasible as detection aperture. For a high value of the objective aperture $\sin\gamma_1$, close to unity, the value of σ will rather be found in the interval $0<\sigma<1$ and the coherence region in the object plane will be approximately equal or larger than the point-spread function of the objective lens. This implies that high-aperture imaging will have a tendency to become more coherent. And, the other way around, strongly incoherent imaging is only possible when the point-spread function of the objective is large with respect to the coherence region in the object plane ($\sigma = \sin\gamma_d/\sin\gamma_1 \gg 1$).

2.3. *Normalized intensity $I_c(0)$ derived from the detector **D***

With the aid of the expressions for $I(q)$ and $I(p, q)$ in Eqs. (4) and (6) I can integrate the far-field intensity produced by the knife-edge over the detection areas for the 1D and 2D case. To have a proper normalization, I divide the integrated intensity by the incident power on the detector in the absence of a knife-edge object. For the 1D case, this normalizing value equals 2σ with a maximum value of 2; for the 2D case it is $\pi\sigma^2$ with π as maximum value when σ exceeds the value of 1. I had already pointed out the normalized values $I_c(0)$ of 1/4 for fully coherent illumination ($\sigma \to 0$) and 1/2 for fully incoherent illumination with $\sigma \to \infty$. And the value of 1/3 is available, thanks to Zernike, for $\sigma = 1$. This σ-value of 1 is quite important in practice, for instance when a mirror system with unit magnification is used, or when high aperture values are used in both the imaging and the illumination part of an imaging system. The common σ value for optical disc read-out is also equal to 1.

2.3.1. 1D geometry

As a function of the incoherence factor σ, the central intensity $I_c(0)$ follows from Eq. (4) and is given by

$$I_c(0) = \frac{1}{2\sigma}\int_{-\sigma}^{+\sigma}\frac{1}{4}\left\{\mathrm{rect}\left[\frac{q}{2}\right] + \frac{1}{\pi^2}\ln^2\left(\frac{1+q}{1-q}\right)\right\}\mathrm{d}q\,, \quad \sigma \le 1, \tag{7a}$$

OPTICS CONTINUUM

$$I_c(0) = \frac{1}{3} + \frac{1}{\pi^2}\int_1^{+\sigma} \frac{1}{4}\ln^2\left(\frac{q+1}{q-1}\right) \mathrm{d}q, \quad \sigma>1\,. \tag{7b}$$

The factor $1/\pi^2$ in front of the integral in Eq. (7b) follows from the fact that I have to evaluate the integral twice (for negative and positive q-values with equal result) but this factor of 2 coming from the second integral is then canceled by the normalization factor of 2. The factor $1/3$ in the same equation for $I_c(0)$ follows from Zernike's result for the integration of the $\ln^2$-function divided by $4\pi^2$ from $\sigma = -1$ to $\sigma = +1$ in Eq. (7a).

The evaluation of the integrals in Eqs. (7a) and (7b) for arbitrary σ-values is performed by me in Appendix A, yielding the 1D results in Eqs. (30) and (36). After the proper normalization according to Eq. (7) and the insertion of the integration limits, I obtain below the values for the central intensity $I_c(0)$ for the cases with a detection area in linear measure of $\sigma \le 1$ and $\sigma>1$, respectively,

$$\begin{aligned} I_c(0) =& \frac{1}{4} + \frac{1}{2\sigma\pi^2}\left[\frac{1}{2}\left\{\left[\ln^2\left(\frac{1+\sigma}{2}\right) - \ln^2\left(\frac{1-\sigma}{2}\right)\right] + \sigma\left[\ln\left(\frac{1+\sigma}{2}\right) - \ln\left(\frac{1-\sigma}{2}\right)\right]^2\right\}\right. \\ & \left. -\mathrm{Sp}\left(\frac{1+\sigma}{2}\right) + \mathrm{Sp}\left(\frac{1-\sigma}{2}\right)\right], \qquad \sigma \le 1, \end{aligned} \tag{8}$$

$$I_c(0) = \frac{1}{2} + \frac{1}{\pi^2}\left[\frac{1}{4}(\sigma+1)\,\ln^2\left(\frac{\sigma+1}{\sigma-1}\right) + \mathrm{Sp}\left(\frac{\sigma+1}{\sigma-1}\right)\right], \qquad \sigma>1. \tag{9}$$

The Spence function $\mathrm{Sp}(x)$ is a variant of the dilogarithm function $\mathrm{Li}_2(x)$, [14]- [15], with the relation $\mathrm{Li}_2(x) = \mathrm{Sp}(1-x)$. Zernike's result of $1/3$ follows from Eq. (8) by taking the limit of $I_c(0)$ for $\sigma \to 1$ and then using that $\mathrm{Sp}(0) = \mathrm{Li}_2(1) = \pi^2/6$ and $\mathrm{Sp}(1) = 0$.

2.3.2. 2D geometry

In Fig. 3(c) a circular detection area has been sketched with a dashed rim, centered at C_D, with a radius $\sigma<1$. One observes that beyond the value $p = 1$, no diffracted light is present in the far-field of the knife-edge. The diffraction in the vertical direction shows contours that closely resemble the straight contours of the 1D geometry in Fig. 3(b). An intensity integration using polar coordinates would accommodate well the circular disk shape, but the intensity variations along vertical lines suggest an integration along the Cartesian coordinates (p, q). I first consider line integrals $I_{int}(p)$ with integration variable q along linear strips with a constant value of p and a length given by $|q| \le \sqrt{\sigma^2 - p^2}$. In a second step I complete the integration by means of the horizontal variable p, running from $-\sigma$ to $+\sigma$. The case with $\sigma = 1$ is considered first .

2D case, $\sigma = 1$

Using Eq. (7a) I find for $\sigma = 1$,

$$I_{int}(p) = \frac{1}{4}\int_{-\sqrt{1-p^2}}^{+\sqrt{1-p^2}} \mathrm{d}q + \frac{1}{\pi^2}\int_{-\sqrt{1-p^2}}^{+\sqrt{1-p^2}} \frac{1}{4}\ln^2\left(\frac{\sqrt{1-p^2}+q}{\sqrt{1-p^2}-q}\right)\mathrm{d}q\,. \tag{10}$$

I then scale the variable q according to $u = q/\sqrt{1-p^2}$ and obtain the expression,

$$\begin{aligned} I_{int}(p) =& \frac{1}{2}\sqrt{1-p^2} + \frac{\sqrt{1-p^2}}{\pi^2}\int_{-1}^{+1} \frac{1}{4}\ln^2\left(\frac{1+u}{1-u}\right)\mathrm{d}u \\ =& \frac{\sqrt{1-p^2}}{2}\left\{1 + \frac{2}{\pi^2}\cdot\frac{\pi^2}{6}\right\} = \frac{2}{3}\sqrt{1-p^2}\,. \end{aligned} \tag{11}$$

OPTICS CONTINUUM

The integration over the variable p then yields the integrated intensity I_p according to

$$I_p = \int_{-1}^{+1} \frac{2}{3}\sqrt{1-p^2}\,\mathrm{d}p = \frac{\pi}{3}\,. \tag{12}$$

To obtain the normalized value $I_c(0)$, I divide I_p by $\pi\sigma^2$ which in this case yields the value $I_c(0) = 1/3$. A value of 0.3333 for the 2D-case was given in [16], as a result of numerical integration of another relevant set of diffraction integrals given in [11].

General 2D case for σ<1

The expression for $I_{int}(p)$ of Eq. (10) is now given by

$$I_{int}(p) = \frac{1}{4}\int_{-\sqrt{\sigma^2-p^2}}^{+\sqrt{\sigma^2-p^2}} \mathrm{d}q + \frac{1}{\pi^2}\int_{-\sqrt{\sigma^2-p^2}}^{+\sqrt{\sigma^2-p^2}} \frac{1}{4}\ln^2\left(\frac{\sqrt{1-p^2}+q}{\sqrt{1-p^2}-q}\right)\mathrm{d}q\,, \qquad |q|<\sigma\,. \tag{13}$$

With the same scaling operation $u = q/\sqrt{1-p^2}$ as for the case $\sigma = 1$ one obtains

$$I_{int}(p) = \frac{1}{2}\sqrt{\sigma^2-p^2} + \frac{\sqrt{1-p^2}}{\pi^2}\int_{-\sigma(p)}^{+\sigma(p)} \frac{1}{4}\ln^2\left(\frac{1+u}{1-u}\right)\mathrm{d}u\,, \quad \text{with} \quad \sigma(p) = \sqrt{\frac{\sigma^2-p^2}{1-p^2}}\,. \tag{14}$$

I use the notation $s = \sqrt{\sigma^2-p^2}$ and $t = \sqrt{1-p^2}$ and then obtain after some rearrangement for $I_{int}(p)$ with the aid of Eqs. (26a) and (30),

$$\begin{aligned} I_{int}(p) =& \frac{s}{2} + \frac{t}{\pi^2}\int_{-s/t}^{+s/t} \frac{1}{4}\ln^2\left(\frac{1+u}{1-u}\right)\mathrm{d}u \\ =& \frac{s}{2} + \frac{1}{2\pi^2}\left[t\left\{\ln^2\left(\frac{t+s}{2t}\right) - \ln^2\left(\frac{t-s}{2t}\right)\right\} + s\left\{\ln\left(\frac{t+s}{2t}\right) - \ln\left(\frac{t-s}{2t}\right)\right\}^2\right] \\ &+ \frac{t}{\pi^2}\left\{\mathrm{Sp}\left(\frac{t-s}{2t}\right) - \mathrm{Sp}\left(\frac{t+s}{2t}\right)\right\}\,. \end{aligned} \tag{15}$$

The value of $I_c(0)$ then follows by integration of Eq. (15) over p and division by $\pi\sigma^2$, which is proportional to the incident radiation on the knife-edge,

$$I_c(0) = \frac{1}{\pi\sigma^2}\int_{-1}^{+1} I_{int}(p)\,\mathrm{d}p\,. \tag{16}$$

Apart from the first term $s/2$ of $I_{int}(p)$ in Eq. (15), no further analytic integration seems possible for $I_c(0)$. I have to conclude that the 1D analytic results were only useful in the first integration step of the 2D case, with respect to the variable q. The second and third terms of Eq. (15) contain logarithmic and dilogarithmic functions which basically have anti-derivatives, but their complicated arguments lead to an impasse in the integration. Fortunately, the integrand $I_{int}(p)$ is, apart from the case $\sigma = 1$, a continuous analytic function. This property enables more sophisticated numerical integration methods, such as Gaussian quadrature, with an important gain in computation speed and numerical accuracy.

General 2D case for σ>1

To find the integral $I_{int}(p)$ for values of σ>1, I take the result of Eq. (11) and then use Eq. (6) twice to cover the full integration range for q from $-\sqrt{\sigma^2-p^2}$ to $+\sqrt{\sigma^2-p^2}$,

$$I_{int}(p) = \frac{2}{3}\sqrt{1-p^2} + \frac{2}{\pi^2}\int_{\sqrt{1-p^2}}^{+\sqrt{\sigma^2-p^2}} \frac{1}{4}\ln^2\left(\frac{q+\sqrt{1-p^2}}{q-\sqrt{1-p^2}}\right)\mathrm{d}q\,, \qquad |q|<\sigma\,. \tag{17}$$

OPTICS CONTINUUM

I now make the change of variable $q = u\sqrt{1-p^2}$ and obtain

$$\begin{aligned} I_{int}(p) =& \frac{2}{3}\sqrt{1-p^2} + \frac{2}{\pi^2}\sqrt{1-p^2}\int_1^{\sqrt{\sigma^2-p^2}/\sqrt{1-p^2}} \frac{1}{4}\ln^2\left(\frac{u+1}{u-1}\right)\mathrm{d}u \\ =& 2\sqrt{1-p^2}\left[\frac{1}{3} + \frac{1}{\pi^2}\int_1^{\sigma'} \frac{1}{4}\ln^2\left(\frac{u+1}{u-1}\right)\mathrm{d}u\right], \end{aligned} \tag{18}$$

with σ' given by $\sqrt{\sigma^2-p^2}/\sqrt{1-p^2} = s/t$.

The expression between square brackets above is identical to the expression of Eq. (7b) and its value is given by $I_c(0)$ in Eq. (9) for the 1D case; one obtains the result

$$I_{int}(p) = 2\sqrt{1-p^2}\left\{\frac{1}{2} + \frac{1}{\pi^2}\left[\left(\frac{\sigma'+1}{4}\right)\ln^2\left(\frac{\sigma'+1}{\sigma'-1}\right) + \mathrm{Li}_2\left(\frac{-2}{\sigma'-1}\right)\right]\right\}. \tag{19}$$

Using the symbols s and t as before in Eq. (15), I obtain the expression

$$I_{int}(p) = 2t\left\{\frac{1}{2} + \frac{1}{\pi^2}\left[\left(\frac{s+t}{4t}\right)\ln^2\left(\frac{s+t}{s-t}\right) + \mathrm{Sp}\left(\frac{s+t}{s-t}\right)\right]\right\}. \tag{20}$$

The central intensity is $I_c(0)$ for the 2D case is then given by

$$I_c(0) = \frac{1}{\pi}\int_{-1}^{+1} I_{int}(p)\,\mathrm{d}p\,. \tag{21}$$

For this second integration step with respect to the variable p, I arrive at the same conclusion as before for the 2D case with $\sigma<1$. The 1D analytic results have enabled the analytic integration over the variable q in the 2D case, but the second integration step with respect to p requires a numerical solution. As it was already mentioned for the 2D case with $0<\sigma<1$, the numerical integration required for $I_c(0)$ profits from the availability of the analytic function $I_{int}(p)$ of Eq. (20) and a Gauss quadrature method can be applied.

3. Knife-edge imaging in the discrete Fourier domain

In this section I assume that the object function is periodic and that the object Fourier transform can be written as a (truncated) series of harmonic components with its appropriate coefficients. One has a sampled version of the continuous Fourier transform. The Fourier series approach has clear advantages in the case of partially coherent imaging, where linearity in amplitude or intensity of the imaging process is absent; convolution integrals in the Fourier domain [18], typical for partially coherent imaging, can be avoided in this way. For that reason, even non-periodic objects are made periodic by so-called *periodic continuation* to allow Fourier domain calculations. For a general 2D object, by means of the periodic continuation of an object with a limited size of $d_{x,n} \times d_{y,n}$, one can write the transmission function of such an object as a Fourier series,

$$t_0(x_n, y_n) = \sum_{m_1}\sum_{m_2} c_{m_1,m_2}\,\exp\{i2\pi[m_1\,u_{x,n}x_n + m_2\,u_{y,n}y_n]\}, \tag{22}$$

where $u_{x,n} = 1/d_{x,n}$ and $u_{y,n} = 1/d_{y,n}$ are the normalized spatial frequencies present in the periodic function $t_0(x_n, y_n)$. As it was stated before, the distance used for normalization in the object plane is the diffraction unit $\lambda/\sin\gamma_1$. The normalized frequencies $(u_{x,n}, u_{y,n})$ are thus given by $(u_x, u_y)\lambda/\sin\gamma_1$. A frequency pair $(m_1 u_{x,n}, m_2 u_{y,n})$ is then a general harmonic component of the Fourier-transformed 2D object function.

Zernike's auxiliary scheme of Fig. 2 will be used again to calculate the central image intensity. For non-periodic objects, the framework for the calculation of e.g. the central intensity in the

OPTICS CONTINUUM

Fourier domain is given in text books such as [17], p. 599-606, [18], p. 312-320 and [19], p. 697-699. The frequency transfer of the object spectrum towards the image plane is governed by a so-called *cross-correlation coefficient* or *transmission cross-coefficient*. These coefficients are convolution-type integrals that depend only on the properties of the pupil of the imaging lens and on the incoherence factor σ of the illumination. If the object function is periodic (or has been made periodic on purpose), the convolution integral reduces to the products of discrete Fourier series associated with the pupil of the lens imaging system and the illumination aperture. In general, it can be stated that this approach provides a very important reduction in computation time.

3.1. Fourier series of a periodic object and frequency transfer towards the image plane

A periodic object is constructed in the object plane O_1, see Fig. 4. The basic function is an infinitely repeated rectangle function with (normalized) period $d_{y,n}$. It creates a sequence of well-separated knife-edge functions with 'uphill' and 'downhill' transients. The structure is invariant in the x_n-direction and unbounded in the y_n-direction. In between, there are downward transients, at a distance $d_{y,n}/2$ from the upward transients.

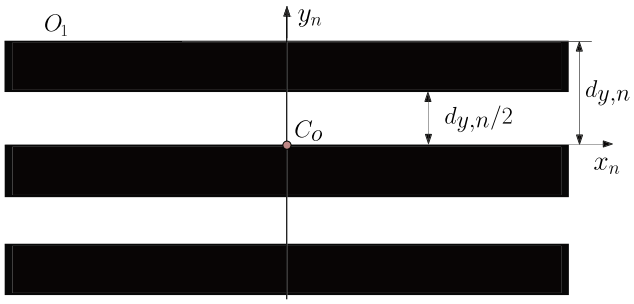

Fig. 4. Graph of the periodic object in the y_n-direction with normalized period $d_{y,n}$ and discrete transmission values of 1 and 0 (duty cycle is 0.5) .

The Fourier coefficients c_m of such a one-dimensional structure are given by

$$c_m = \frac{1}{2}\exp\left(\frac{i\pi m}{2}\right)\operatorname{sinc}\left(\frac{\pi m}{2}\right). \tag{23}$$

With the aid of Fig. 5 I now illustrate the calculation of the integrated intensity in the detector plane. In the left drawing a), part of the periodically continued knife-edge object has been shown in the object plane with its center at C_o. A transition from 0 to 1 is found at the vertical coordinate $y_n = 0$ in the point C_o. Two nonzero diffracted orders, blue and green in the drawing, are projected in the far-field of the periodic object, on the curved surface Σ_1; the zero order extends over the dashed circular disk with red color. In drawing b), with the aid of a collector lens, the diffraction orders have been projected on the planar detector surface D. The light collection area D_σ of the detector is also shown, delimited by the black circle with radius σ (center at C_D). In general, taking into account a possible shift of the periodic object in the y_n-direction over a distance $\Delta_{y,n}$, one obtains for the integrated intensity over the detection area D_σ,

$$I(\Delta_{y,n}) = \sum_{m=-m_{max}}^{+m_{max}} |c_m|^2\, D(u_{y,n}; m, m) + 2\Re\left\{\sum_{M=1}^{2m_{max}} \sum_{m=-m_{max}+M}^{+m_{max}} \exp\left[i2\pi M u_{y,n}\Delta_{y,n}\right] \times\ c_m\, c^*_{m-M}\, D(u_{y,n}; m, m-M)\right\}. \tag{24}$$

OPTICS CONTINUUM

I derive the expression for the integrated intensity on the detector area D_σ in Appendix B.

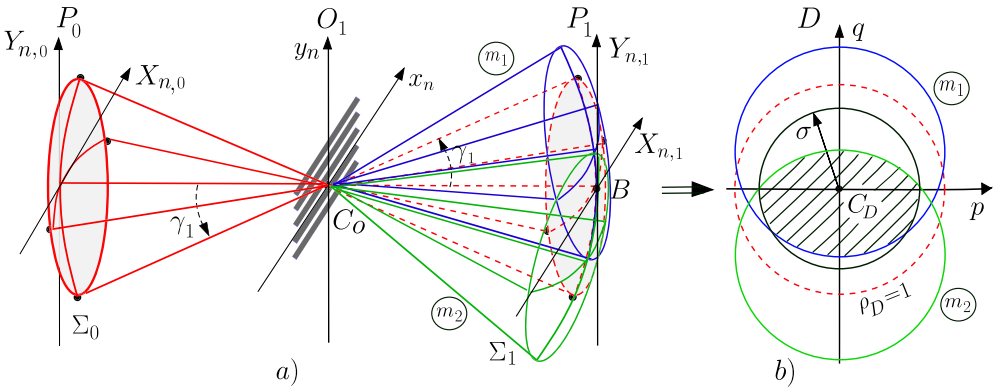

Fig. 5. a) Illustrating the interference of two nonzero diffraction orders (m_1 and m_2); the diffraction orders are produced by the one-dimensional periodic object with normalized frequency $u_{y,n}$ in the object plane O_1. b) Calculation in the detector plane D of a cross-correlation coefficient $D(u_{y,n}; m_1, m_2)$.

The first term of the integrated intensity $I(\Delta_{y,n})$ is the sum of the integrated intensities in the detector plane D produced by all the individual diffraction orders of the periodic knife-edge object. These intensities lead to the background intensity on the detector. In the second term of $I(\Delta_{y,n})$ one has to sum all the integrated intensities produced by any pair of interfering diffracted orders with different indices m and $m - M$. This summation leads to intensity contributions on the detector that are associated with the M-th spatial harmonic of the periodic object that is present in the integrated intensity when the periodic object is laterally shifted in the y_n-direction.

In the first term of $I(\Delta_{y,n})$ the summation is performed over a symmetric range of m, running from $-m_{max}$ to $+m_{max}$. The maximum normalized frequency $u_{y,n,max}$ that can be transferred by an imaging system amounts to $(1 + \sigma)$ if $\sigma \leq 1$ and is limited to 2 for $\sigma > 1$. The frequency transfer at a specific spatial frequency is weakened by the limited collection area D_σ with its characteristic diameter 2σ. All these effects have been incorporated in the general Fourier cross correlation coefficient $D(u_{y,n}; m_1, m_2)$.

In Fig. 6, for a one-dimensional knife-edge object, the calculation of such cross-correlation coefficients $D(u_{y,n}; m_1, m_2)$ is geometrically illustrated for an ideal two-dimensional optical system with circular symmetry. The difference in spatial frequency between two diffraction orders D_1 and D_2 is $(m_1 - m_2)u_{y,n} = Mu_{y,n}$. From Fig. 2, one observes that the coordinates of the midpoints of each diffraction order on the detector surface D are given by $(p, q) = (0, m_1 u_{y,n})$, point M_1, and by $(p, q) = (0, m_2 u_{y,n})$, point M_2. The radius ρ of each diffraction order is equal to the normalized value of unity, corresponding to the radius of the objective aperture P_0. In the case of aberration-free optics and uniform illumination of the pupil surface P_0, the value of $D(u_{y,n}; m, m - M)$ can be analytically calculated. Figure 6 shows that the size of each shaded overlap area follows from the overlap area of two diffraction orders with unit radii, to the extent that this area falls within the source circle D_σ with radius σ. In graph a) the incoherence factor σ is smaller than 1 and $D(u_{y,n}; m, m - M)$ has to be normalized with respect to the area $\pi\sigma^2$ of the circle D_σ. In graph b) the incoherence factor σ is larger than 1 and the normalization factor is π, the area of the diffraction orders D_1 or D_2. For an ideal 1D or 2D imaging system with rectangular or circular geometry, I analytically calculate values for $D(u_{y,n}; m, m - M)$ for any combination of the values of m and M; numerical 2D integration of the common area of three circles is not required. An analytic formula for the overlap area of two circles with equal radii and a third circle with a different radius can be obtained from [19], page 679. For a 1D

OPTICS CONTINUUM

imaging system the three circles in Fig. 6 should be replaced by one-dimensional 'bands' with the corresponding heights of 2 or 2σ. The value of a coefficient $D(u_{y,n}; m, m-M)$ then follows from the normalized height of the overlap region measured along the y_n-direction.

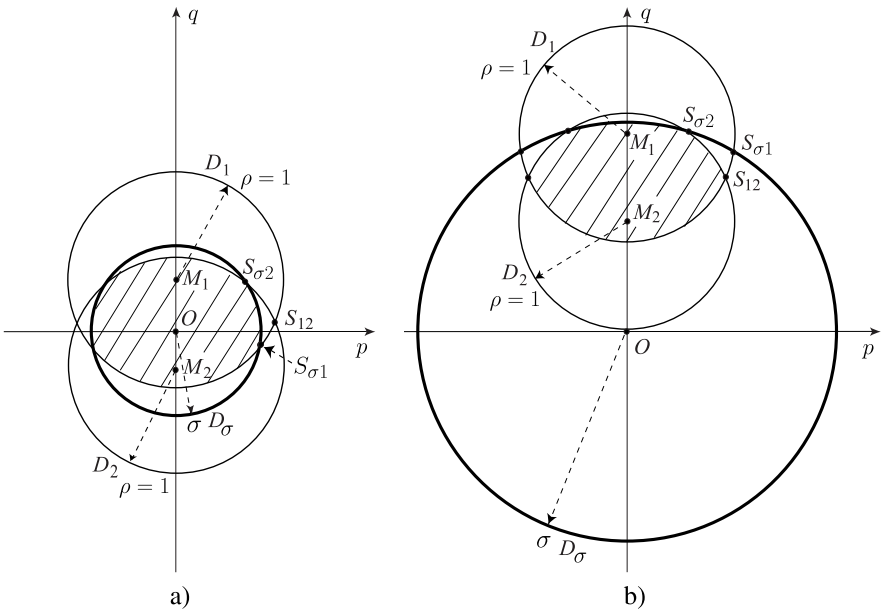

Fig. 6. Illustrating the calculation of the value of a cross-correlation coefficient $D(u_{y,n}; m_1, m_2)$ for a one-dimensional periodic object with period $d_{y,n}$. The value of such a coefficient $D(u_{y,n}; m_1, m_2)$ equals the hatched common area of three circles. For the physical background of graphs a) and b) the reader is referred to Appendix B.

For the calculation of the central intensity $I_c(0)$ corresponding to zero object shift ($\Delta_{y,n} = 0$), Eq. (24) can be further simplified and given by

$$I_c(0) = \sum_{m=-m_{max}}^{+m_{max}} |c_m|^2 \; D(u_{y,n}; m, m) + 2\Re\left\{ \sum_{M=1}^{2m_{max}} \sum_{m=-m_{max}+M}^{+m_{max}} c_m \, c^*_{m-M} \, D(u_{y,n}; m, m-M) \right\}. \qquad (25)$$

For the central intensity $I_c(0)$, only positive even values of M need to be considered since all odd frequency components have zero amplitude for $\Delta_{y,n} = 0$ (the odd coefficients c_m are purely imaginary). For an off-axis vertical position of the knife-edge transition, one should include the odd harmonic components, among others when computing the complete edge response. The number m_{max} in Eq. (25) is given by the maximum number of overlapping diffracted orders that, entirely or partly, are incident on the circular detector with effective detection area D_σ.

The results of this section on Fourier imaging of a knife-edge will be used to show the convergence of the value of $I_c(0)$ towards the values that have been calculated in subsection 2.1 using Zernike's detection scheme according to Fig. 2 in the *spatial* domain. In particular, I will show how the Fourier result converges towards the analytic value of $I_c(0)$ when the periodic continuation distance $d_{y,n}$ takes on large values; unfortunately, at the cost of a quadratically increasing computational effort.

OPTICS CONTINUUM

4. Results for $I_c(0)$ and the edge response obtained from calculations in the spatial and in the Fourier domain

In this section, I first discuss the accuracy and the efficiency (calculation time) of the various approaches to calculate the central intensity $I_c(0)$ in the image plane of a centered knife-edge. As before, I will use the scheme of Fig. 2 to perform the calculation of the integrated intensity on the detector D with a radial extent of σ. In Subsection 2.1 I have obtained $I_c(0)$ by means of calculations in the spatial domain, using normalized coordinates (p, q). The results for $I_c(0)$ are denoted by $I_{1,S}$ and $I_{2,S}$, respectively, depending on their values in a 1D or a 2D optical system. The function $I_{1,S}$ for a 1D system can be considered to be exact, of the order of 10^{-12} in double-precision calculation or less. The values of $I_{2,S}$ for a 2D system are obtained by means of a numerical integration over the horizontal variable p on the detector (see Fig. 2(c)). If one would apply for instance a trapezium rule or Simpson's rule, one typically needs 10^6 function evaluations to achieve the same error of 10^{-12}. Knowing that an analytic function is available, a Gauss-quadrature scheme with non-equidistant sample points can be used for integration. It turns out that for the relatively smooth functions of p to be integrated, a Gauss-quadrature scheme with 8 or 10 sample points and typically 200 to 300 required function evaluations is adequate to achieve the same relative error of 10^{-12}. I thus conclude that the numerically obtained 2D results have a precision that is comparable to the associated 1D analytic results with a strongly reduced computational effort. The calculations in the Fourier domain, see section 3, Eq. (25), have given the comparable results $I_{1,F}$ and $I_{2,F}$, where I have used the appropriate cross-correlation coefficients $D(u_{y,n}; m, m-M)$ for a 1D or a 2D optical system. The calculation of the cross-correlation coefficients for the 1D case is rather straightforward. The calculation of the same coefficients for the 2D case has been illustrated in Fig. 6. The cross-correlation coefficients $D(u_{y,n}; m, m-M)$ have exact values for an aberration-free optical system that is illuminated by a planar or spherical wave with uniform amplitude. The accuracy of the calculated intensities $I_{1,F}$ and $I_{2,F}$ also depends on the period $d_{y,n}$ that has been used for the periodic continuation of the rectangular object function, of which the rising edge at $y_n = 0$ is relevant. A small value of $d_{y,n}$ gives rise to aliasing effects and will introduce an offset with respect to the $I_c(0)$-value of an isolated knife-edge.

4.1. Calculation of $I_c(0)$

In Table 1 I have printed, for three representative values of σ, the results for $I_c(0)$ in the 1D and 2D geometry, obtained either from the spatial domain or from the Fourier domain. In Table 1 one observes that the Fourier values $I_{1,F}$ and $I_{2,F}$ converge to the exact values given by $I_{1,S}$ and $I_{2,S}$ if the number $(1+\sigma)/u_{y,n} = (1+\sigma)d_{y,n}$ (with a maximum of $2d_{y,n}$) of transferred components in the Fourier spectrum of the knife-edge is increased by choosing larger values for $d_{y,n}$. Roughly speaking, for a $d_{y,n}$-value of 10 diffraction units $\lambda/\sin\gamma_1$, the Fourier values show relative errors in the range from 0.005 (low σ-values) down to 0.00015 for the larger σ-values. The lower precision for more coherent detection is explained by the smaller frequency pass-band of the optics. For $d_{y,n} = 100$, the relative errors range from 4.10^{-5} to 10^{-6}. And, finally, for $d_{y,n} = 1000$, the error reaches values between 3.10^{-7} to 2.10^{-8}. I conclude that for most practical applications, a value of $d_{y,n}$ of the order of 100 will be sufficient.

On average, the lowest errors are obtained for the 2D geometry. I also observed that for low values of $d_{y,n}$, a small change of its value can cause relatively large changes in the detected intensity. This is explained by the discrete appearance or disappearance of frequency components in the transmitted spectrum by the imaging system, especially at low σ-values.

In Fig. 7 I have plotted sets of collected data for $I_c(0)$ in the 1D and the 2D case. At the σ-scale of the graph, one encounters the special cases of $1/4$ and $1/3$ for σ is 0 or 1. The limiting value of $1/2$ is reached for very large σ-values, e.g. for the 2D case one has that $I_c(0) = 0.498280$ at $\sigma = 50$, and 0.499914 for $\sigma = 1000$. Such incoherence factors have no practical relevance, since

OPTICS CONTINUUM

Table 1. Central intensities $I_{1,F}$ and $I_{2,F}$ as a function of σ and the periodic-continuation distance $d_{y,n}$. Numerical comparison with the exact/accurate values of $I_{1,S}$ and $I_{2,S}$.

		Fourier results compared with exact values of $I_c(0)$			
σ	$d_{y,n}$	$I_{1,F}$	$I_{1,S}$	$I_{2,F}$	$I_{2,S}$
0.6	10	0.2653914046	0.2643610760	0.2618364489	0.2612424126
	100	0.2643717576		0.2612459557	
	1000	0.2643611828		0.2612424418	
1.0	10	0.3338098919	1/3	0.3332738943	1/3
	100	0.3333410193		0.3333324012	
	1000	0.3333334394		0.3333333221	
2.5	10	0.4579587504	0.4579133254	0.4638575582	0.4639320694
	100	0.4579129641		0.4639310695	
	1000	0.4579133218		0.4639320595	

the lateral resolution in the image will be strongly reduced. For that reason the graph has been limited to $\sigma = 3.0$ with $I_c(0) = 0.470394$ (2D case).

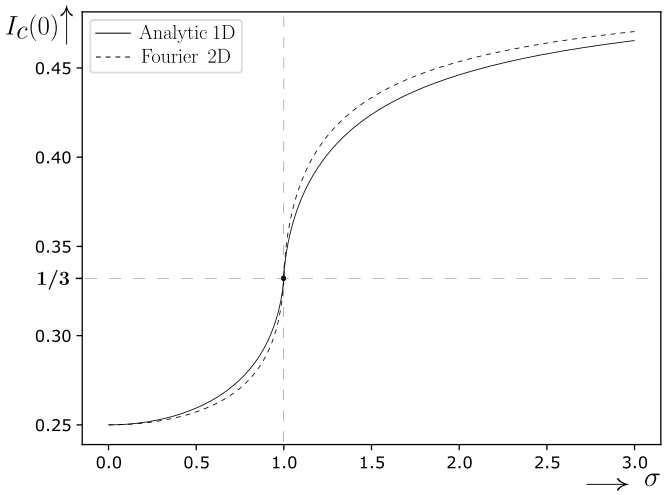

Fig. 7. The central intensity $I_c(0)$ in the image of a knife-edge as a function of the incoherence factor σ in the illuminating beam. The solid curve uses the 1D analytic result; the dashed curve has been calculated for the 2D case using Fourier analysis.

4.2. Calculation of the edge response

I finish this section with a graph (Fig. 8) showing the edge response of an optical system as a function of the σ-value of the system, both for a 1D and a 2D system. I have used the Fourier domain for the calculation since it offers a very efficient method to obtain the changing value of $I_c(0)$ as a function of the position shift Δy_n of the knife edge. From the Fourier coefficients the edge response is obtained by simple multiplications with sines and cosines having their appropriate harmonic arguments. And, as many authors have stated before, the cross-correlation coefficients are proper to the imaging system itself and do not have to be recalculated if only the optical transmission or reflection function of the object changes without a modification of the

OPTICS CONTINUUM

period $d_{y,n}$. Concerning computing time, the calculation of all the cross-correlation coefficients $D(u; n, m)$ took 0.3 s for $d_{y,n} = 10$, 3.5 s for $d_{y,n} = 100$ and 100 s for $d_{y,n} = 1000$. For comparison, the calculation of a single intensity value $I_c(0)$ in the spatial domain (2D geometry) typically takes 0.001 s. The difference between the 1D and 2D curves in Fig. 8 is hardly perceptible if the incoherence factor is as small as $\sigma = 0.2$. The reason is that the optical transfer function for both cases is mainly unity at such a low σ-value. The 1D and 2D curves for larger σ-values show differences in both the shadow and the open zone. As I concluded earlier, their crossings of the exact shadow position at $y_n = 0$ are rigorously coincident when $\sigma = 1$. For $\sigma = 2.5$, the 1D and 2D curves intersect each other at a slightly negative value of y_n in the open zone. The figure also shows that the 1D edge response is systematically steeper than its 2D equivalent. This can be explained by the smaller half-width in the spatial domain of a 1D point-spread function as compared to its 2D counterpart.

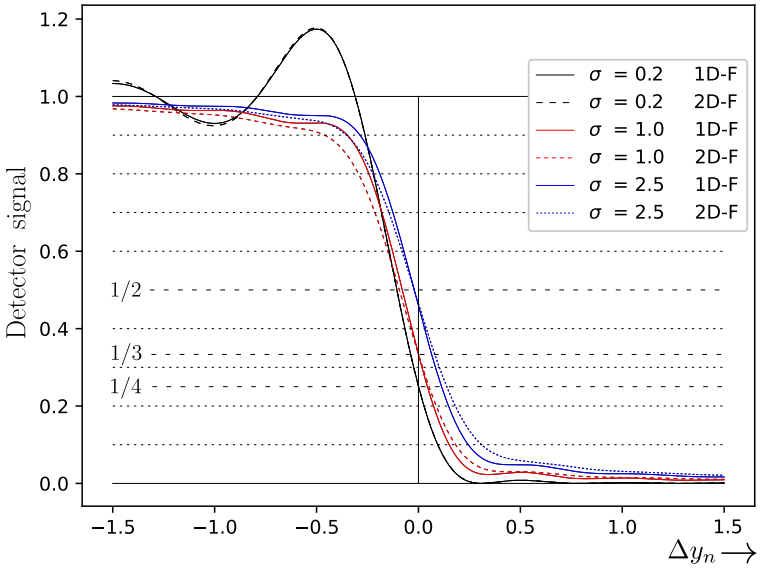

Fig. 8. The edge response when laterally scanning a knife-edge through optimum focus in Zernike's auxiliary set-up, for a 1D and 2D geometry. Parameter is the incoherence factor σ (calculations in the Fourier domain, by executing successive shifts Δy_n of the knife-edge in the object plane).

5. Conclusion

I have obtained analytic values for the central intensity of a knife-edge image produced by an ideal 1D imaging system for an arbitrary value of the incoherence factor σ. I have also implemented this 1D result in the calculation of the same central intensity for a 2D imaging system. I have demonstrated that the same analytic value of $1/3$ was obtained for both imaging systems if $\sigma = 1$, a new result to my knowledge. I could also show that the numerical calculation of the central intensity in a 2D system is greatly facilitated by using my 1D analytic result and that I was thus able to achieve a strong reduction in calculation time and gain in accuracy.

My previous results where obtained by calculations in the spatial domain. In general, calculations in the Fourier domain are frequently used for solving optical problems. For the calculation of the edge response of an optical system I used the formalism of Fourier optics by periodic continuation (period $d_{y,n}$) of a rectangular function. I then compared my exact 1D results (spatial domain) for the central intensity with the same quantities obtained via my Fourier method.

OPTICS CONTINUUM

In the perfect optical systems under consideration, I obtained exact values of the cross-correlation coefficients in the Fourier domain. The differences between the two approaches then depend only on the repetition distance $d_{y,n}$ in the Fourier approach. I could conclude that a repetition distance of $d_{y,n}$, equal to typically 100 diffraction units $\lambda/\sin\gamma_1$ in the object plane, is sufficient to obtain an accuracy ϵ of 10^{-5}. For the value $d_{y,n} = 100$, the descending edge of interest is accompanied by raising edges at distances of 50 diffraction units (see Fig. 4). The accuracy ϵ is related to the sampling density in the Fourier pass-band. Its value is well approximated by my expression $\epsilon = d_{y,n}^{-2}/10 = u_{y,n}^{2}/10$.

Finally, from the calculated edge responses I observed that, as expected, the 1D and 2D responses intersect each other exactly at the geometrical position of the edge if $\sigma = 1$. For values $\sigma>1$, the 1D and 2D edge responses intersect each other at a position that is slightly shifted towards the 'open' part of the edge response. Manipulation of the shape and the size of the objective and detector aperture thus yield a possibility to modulate the position of the edge response without explicit mechanical movement of the object, a subject for further research in the field of precision metrology.

Regarding the applicability of the edge response findings in this paper, precision metrology with a knife-edge, with an absorptive or transmissive slit or with a curved edge could be mentioned. Of course, because of the scalar diffraction assumption, there is a limit with respect to the convergence angles in the imaging optics. Fortunately, in microscopy and optical lithography/metrology, there is a tendency to use shorter wavelengths ($\lambda = 13$ nm) and a somewhat reduced aperture (≈ 0.5); the scalar diffraction model can still be used in this context.

A. Evaluation of two integrals (1D geometry)

In this Appendix I evaluate the two integrals that are needed to calculate the integrated optical intensity $I_c(0)$ on the far-field detector D in Fig. 2. I consider a 1D imaging geometry with an intensity variation on the detector as a function of the coordinate q according to Fig. 3(b). The normalized central intensity $I_c(0)$ is given by Eq. (7). The two basic integrals that have to be evaluated are,

$$\frac{1}{4}\int_{-\sigma}^{+\sigma} \ln^2\left(\frac{1+q}{1-q}\right) \mathrm{d}q\,, \quad 0<\sigma \le 1, \tag{26a}$$

$$\frac{1}{4}\int_{1}^{+\sigma} \ln^2\left(\frac{q+1}{q-1}\right) \mathrm{d}q\,, \quad \sigma \ge 1\,. \tag{26b}$$

A.1. Calculation of the first integral ($0<\sigma \le 1$)

In the integral of Eq. (26a) I introduce the change of variables $y = (1+q)/2$, yielding the expression

$$I_{\sigma<1} = \frac{1}{2}\int_{(1-\sigma)/2}^{(1+\sigma)/2} \left[\ln^2(y) - 2\ln(y)\,\ln(1-y) + \ln^2(1-y)\right] \mathrm{d}y\,. \tag{27}$$

The integrals over the first and the third term of the integrand yield identical values and this leads to the following expression for I,

$$I_{\sigma<1} = \int_{(1-\sigma)/2}^{(1+\sigma)/2} \{\ln(x)\,[\ln(x) - \ln(1-x)]\}\,\mathrm{d}x. \tag{28}$$

OPTICS CONTINUUM

I then proceed with integration by parts and obtain, after some manipulation,

$$\begin{aligned} I_{\sigma<1} =& \int_{(1-\sigma)/2}^{(1+\sigma)/2} [\ln(x) - \ln(1-x)]\, \mathrm{d}\,\{x\,[\ln(x)-1]\} \\ =& x\ln(x)\,\{\ln(x)-1\} - \ln(1-x)\,\{x\ln(x) - x + 1\}\Big|_{(1-\sigma)/2}^{(1+\sigma)/2} \\ &+ \int_{(1+\sigma)/2}^{(1-\sigma)/2} \frac{\ln(1-y)}{y}\mathrm{d}y. \end{aligned} \tag{29}$$

The remaining integral in Eq. (29) is related to the dilogarithmic function [14], denoted by $\mathrm{Li}_2(a) = -\int_0^a \{\ln(1-t)/t\}\,\mathrm{d}t$. I substitute the integration limits in the dilogarithm of Eq. (29) and obtain the expression $\mathrm{Li}_2\{(1+\sigma)/2\} - \mathrm{Li}_2\{(1-\sigma)/2\}$. The dilogarithm $\mathrm{Li}_2(x)$ can be replaced by Spence's function using the relation $\mathrm{Li}_2(a) = \mathrm{Sp}(1-a)$. The insertion of the integration limits in the first term on the right-hand side of Eq. (29) then leads to the final expression,

$$\begin{aligned} I_{\sigma<1} =& \frac{1}{2}\left\{\left[\ln^2\left(\frac{1+\sigma}{2}\right) - \ln^2\left(\frac{1-\sigma}{2}\right)\right] + \sigma\left[\ln\left(\frac{1+\sigma}{2}\right) - \ln\left(\frac{1-\sigma}{2}\right)\right]^2\right\} \\ &- \mathrm{Sp}\left(\frac{1+\sigma}{2}\right) + \mathrm{Sp}\left(\frac{1-\sigma}{2}\right), \end{aligned} \tag{30}$$

where the use of either Spence's function Sp or the dilogarithm function Li_2 is fully arbitrary.

Eq. (30) can also be used to obtain the value of $I_{\sigma<1}$ when σ approaches 1. The first term of Eq. (30) has a limit of zero and $I_{\sigma<1}$ then reduces to the sum of two Spence-functions, such that $I_{\sigma=1} = -\mathrm{Sp}(1) + \mathrm{Sp}(0) = 0 + \pi^2/6$.

A.2. Calculation of the second integral for (σ>1)

The integral in Eq. (26b) is subjected to the change of variables $(q+1)/(q-1) = y+1$ and I obtain the expression

$$I_{\sigma>1} = \frac{1}{2}\int_{2/(\sigma-1)}^{+\infty} \frac{\ln^2(y+1)}{y^2}\mathrm{d}y\,. \tag{31}$$

In Eq. (31) I replace the upper limit $+\infty$ of the integration interval by $+z$ and will then evaluate the integral for z tends to $+\infty$. Integration by parts yields the expression

$$\begin{aligned} I_{\sigma>1} =& \left[-\frac{1}{2}\frac{\ln^2(y+1)}{y}\right]\Bigg|_{2/(\sigma-1)}^{+z} + \frac{1}{2}\int_{2/(\sigma-1)}^{+z} \frac{1}{y}\,\mathrm{d}\left[\ln^2(y+1)\right] \\ =& \frac{1}{4}(\sigma-1)\ln^2\left(\frac{\sigma+1}{\sigma-1}\right) + \int_{2/(\sigma-1)}^{+z} \ln(y+1)\left(\frac{1}{y} - \frac{1}{y+1}\right)\mathrm{d}y\,. \end{aligned} \tag{32}$$

OPTICS CONTINUUM

I now change the sign of the variable y in the integral on the second line of Eq. (32) and obtain

$$\begin{aligned} I_{\sigma>1} &= \frac{1}{4}(\sigma-1)\ln^2\left(\frac{\sigma+1}{\sigma-1}\right) + \int_{-2/(\sigma-1)}^{-z} \frac{\ln(1-y)}{y}\mathrm{d}y + \int_{-2/(\sigma-1)}^{-z} \frac{\ln(1-y)}{(1-y)}\mathrm{d}y \\ &= \frac{1}{4}(\sigma-1)\ln^2\left(\frac{\sigma+1}{\sigma-1}\right) - \mathrm{Li}_2(-z) + \mathrm{Li}_2\left(-\frac{2}{\sigma-1}\right) - \int_{(\sigma+1)/(\sigma-1)}^{+z} \frac{\ln(y)}{y}\mathrm{d}y \\ &= \frac{1}{4}(\sigma+1)\ln^2\left(\frac{\sigma+1}{\sigma-1}\right) - \frac{1}{2}\ln^2(z) - \mathrm{Li}_2(-z) + \mathrm{Li}_2\left(-\frac{2}{\sigma-1}\right). \end{aligned} \tag{33}$$

To deal with the $\ln^2$-function and the dilogarithm with their large arguments $\pm z$ tending to $\pm\infty$, I use the dilogarithm *reflection* formula [14]- [15] which reads for a general argument $-z$,

$$-\mathrm{Li}_2(-z) - \frac{1}{2}\ln^2(z) = \frac{\pi^2}{6} + \mathrm{Li}_2(-1/z). \tag{34}$$

I insert Eq. (34) in Eq. (33), take the limit for $z \to +\infty$ and, knowing that $\mathrm{Li}_2(0) = 0$, I obtain the expression,

$$I_{\sigma>1} = \frac{\pi^2}{6} + \frac{1}{4}(\sigma+1)\,\ln^2\left(\frac{\sigma+1}{\sigma-1}\right) + \mathrm{Li}_2\left(-\frac{2}{\sigma-1}\right), \tag{35}$$

or, alternatively, using Spence's function,

$$I_{\sigma>1} = \frac{\pi^2}{6} + \frac{1}{4}(\sigma+1)\,\ln^2\left(\frac{\sigma+1}{\sigma-1}\right) + \mathrm{Sp}\left(\frac{\sigma+1}{\sigma-1}\right). \tag{36}$$

B. Frequency transfer by a partially coherently illuminated imaging system

In this appendix I will briefly discuss the image formation in a conventional illumination and imaging system. More specifically, I will derive the expressions for the intensity in the image plane according to Eqs. (24) and (25). Figure 9 shows the elements of such an imaging system. The illumination system with its source center at S_o produces a light distribution in the object plane through C_o with a certain limited coherence region in the vicinity of a general object point P. The size and the shape of this coherence region depend on the angular extent γ_d of the source, as seen from the point C_o. The object and image side pupils are found at $C_{o,P}$ and $C_{i,P}$ and have transmission functions $f(Y)$ and $f'(Y')$, respectively.

Starting with the source with its angular extent γ_d, it produces a mutual coherence function $\mu(y)$ in the object plane. According to the van Cittert-Zernike theorem [20]- [21], the mutual coherence function μ is given by the Fourier transform of the intensity function $I_s(Y_s)$ of the source. The lateral size of the source S is scaled with respect to the normalized size of the entrance and the exit pupil; in line with previous notation, the 1D source has a lateral size of 2σ. For a 1D optical system, the functions $f(Y)$ and $f'(Y')$ are given by a rectangle function with width 2 in the Y- and Y'-directions.

For the image formation in a general point $\boldsymbol{P'}$, at the image position of the corresponding object point $\boldsymbol{P}$, the partially coherent intensity contributions at $\boldsymbol{P'}$ by all possible pairs of object points (P_1, P_2) have to be added. And for each pair of object points P_1 and P_2, the local object transmission values $t(y_1)$ and $t(y_2)$ should be taken into account. A *partially* coherent intensity contribution has to be multiplied by the mutual coherence function μ, following from the lateral distance $(y_1 - y_2)$ between a pair of object points P_1 and P_1. In the case of a rectangular shape of the pupil function $f'(Y')$, the complex amplitude impulse response $A(y')$ in the image plane is

OPTICS CONTINUUM

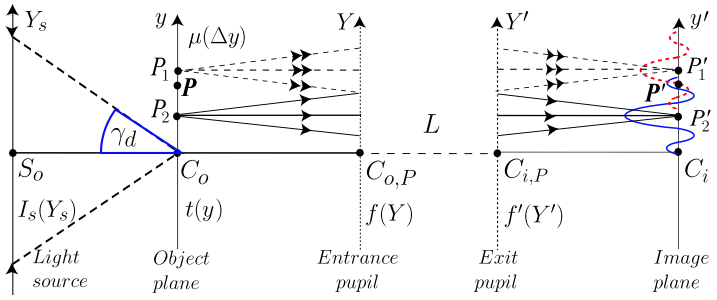

Fig. 9. Schematic drawing of partially coherent image formation by a lens system L. The object plane (center at C_o) is partially coherently illuminated by the source with its center at S_o. The object transmission function is $t(y)$. The image intensity is measured in the plane through C_i. The centers of the entrance and exit pupil are found at $C_{o,P}$ and $C_{i,P}$. The complex amplitude impulse response functions $A(y')$ delivered by the object points P_1 and P_2 have been plotted in blue (solid curve) and red (dashed curve). Normalized coordinates are used in the object / image plane and in the pupil planes.

given by a $\sin(y')/y'$ function. The partially coherent intensity contribution from two points P_1 and P_2 is given by $\mu(y_1 - y_2)\,\{t(y_1)\,A(y' - y_1)\}\,\{t(y_2)A(y' - y_2)\}^*$.

From these considerations it follows that, after integration over all possible positions of P_1 and P_2 in the object plane, the intensity $I(y')$ at a general point $\boldsymbol{P'}$ in the image plane is given by

$$I(y') = \iint_{-\infty}^{+\infty} \mu(y_1 - y_2)\, t(y_1)\, A(y' - y_1)\, t^*(y_2)\, A^*(y' - y_2)\; dy_1 dy_2\,. \tag{37}$$

This equation yields $I(y')$ by computations in the spatial domain. Inspection of the equation shows that it is a double convolution integral with respect to the integration variables y_1 and y_2, coupled by the mutual coherence function $\mu(y_1 - y_2)$. The disadvantage of the oscillations and the wide nonzero range of the impulse response function $A(y')$ complicates the evaluation of this integral. It is worthwhile to see if, by switching from the spatial domain functions to their Fourier counterparts, one can decrease the computational effort. I thus write the spatial domain functions in the integrand of Eq. (37) by means of their Fourier transforms. I obtain the following expressions, together with the Fourier transform $\tilde{I}(Y')$ of the image plane intensity function $I(y')$,

$$\mu(y) = \int_{-\infty}^{+\infty} I_s(Y_1)\, \exp\{-i2\pi y Y_1\}\, dY_1, \qquad t(y) = \int_{-\infty}^{+\infty} \tilde{t}(Y_2)\, \exp\{-i2\pi y Y_2\}\, dY_2, \tag{38}$$

$$A(y) = \int_{-\infty}^{+\infty} f'(Y_3)\, \exp\{-i2\pi y Y_3\}\, dY_3, \qquad \tilde{I}(Y') = \int_{-\infty}^{+\infty} I(y')\, \exp\{-i2\pi y' Y'\}\, dy'\,. \tag{39}$$

The insertion of $I(y')$ of Eq. (37) in the expression for $\tilde{I}(Y')$ of Eq. (39) then yields after some manipulation the expression,

$$\begin{aligned}\tilde{I}(Y') &= \iiiint\!\!\int_{-\infty}^{+\infty} I_s(Y_1)\,\tilde{t}(Y_2) f'(Y_3)\,\tilde{t}^*(Y_4) f'^*(Y_5)\,\delta(Y_1+Y_2-Y_3) \\ &\qquad \times\ \delta(Y_1+Y4-Y_5)\,\delta(Y_3+Y_5-Y')\,dY_1dY_2dY_3dY_4dY_5 \\ &= \iint_{-\infty}^{+\infty} I_s(Y_2-Y_1)\,\tilde{t}(Y_1)\,\tilde{t}^*(Y'+Y_1) f'(Y_2) f'^*(Y'+Y_2)\,dY_1dY_2,\end{aligned} \tag{40}$$

where $\delta(Y)$ is the Dirac delta-function.

I adjust Eq. (40) by the change of coordinates $u_1 = Y_1$, $u_2 = Y_2 - Y_1$, to obtain the result,

$$\tilde{I}(Y') = \iint_{-\infty}^{+\infty} I_s(u_2)\,\tilde{t}(u_1)\,\tilde{t}^*(u_1+Y') f'(u_1+u_2) f'^*(u_1+u_2+Y')\,du_1du_2 \tag{41}$$

The equation is easily extended to a 2D geometry. For a 2D optical system, the functions $I_s(u)$ and $f'(u)$ will be written as $I_s(u,v)$ and $f'(u,v)$, e.g. corresponding to the circular shape encountered in a common condenser or imaging system. In the case of an edge response, the Fourier transform of the function $t(y)$ yields the same 1D result.

Inspection of the integral for $\tilde{I}(Y')$ shows the regions in the (u_1,u_2) integration domain where the integrand contributes zero. For a 2D system, the integrand is zero for a combination of (u_2,v_2)-values such that the length $(u_2^2+v_2^2)^{1/2}$ exceeds the value of σ associated with the extent of the circular source S. For a nonzero integrand value it is required that the product of the two $f'(u,v)$-functions is nonzero, or, geometrically speaking, that the two centers of the circles with unit radius shouldn't have a (normalized) distance larger than 2.

In Fig. 6(a) and 6(b) I have shown two specific cases for the source size σ and for the position of shifted diffracted orders. An order D_1 is shown, corresponding to a pupil function $f'(u_1+u_2)$ and an order D_2, associated with the pupil function $f'(u_1+u_2+(m_2-m_1)u_{y,n})$. The combined effect of source size and positions of diffracted orders leads in Fig. 6 to a hatched overlap area of the three circles. This (normalized) overlap area corresponds to the analog value between 0 and σ of a specific cross-correlation coefficient $D(u_{y,n};m_1,m_2)$ as used in Eqs. (24) and (25). I note that such a coefficient D depends only on the properties of the illumination and imaging system. The special cases of fully coherent or incoherent object illumination follow from Eq. (41) (and Fig. 6) by reducing the radius σ of the source function $I_s(u_2)$ to a point-like circular region or by making it very large.

To reach full agreement between Eqs. (24) and (41), we use the discrete Fourier series of Eq. (22) for the Fourier transforms $\tilde{t}(u_1)$ and $\tilde{t}^*(u_1+Y')$ in Eq. (41). $\tilde{I}(Y')$ is then converted to a summation over a finite number of terms, running from 0 to the highest normalized frequency $u_{max} = 2$ that can be transferred by an optical imaging system. With the knowledge of $\tilde{I}(Y')$ for a (large) number of discrete frequency components $Y'_m = mu_{y,n}$, we then reconstruct the intensity $I(y')$ in the image plane according to the summation scheme of Eq. (24), with Δy_n replaced by the image plane coordinate y' in a conventional imaging system.

At this point, one may state that the integrated detector intensity $I(\Delta y_n)$ of Eq. (24), calculated with the aid of Zernike's auxiliary set-up, is equal to the image plane intensity $I(y')$ that I have derived in this appendix, provided that the normalized coordinates Δy_n and y' have the same value. Of course, this result also follows directly from Welford's general statements about the equivalence of conventional and scanning microscopy in [5].

OPTICS CONTINUUM

Acknowledgement. The author acknowledges stimulating discussions with Dr. A. J. E. M. Janssen of Eindhoven University of Technology, Eindhoven, The Netherlands. In particular, he provided me with an analytic proof in the Fourier series domain of Zernike's factor of $1/3$ for the 1D case at $\sigma = 1$, by means of an adapted version of Eq. (25).

Disclosures. The author declares no conflicts of interest.

Data availability. Data underlying the results presented in this paper are not publicly available at this time but may be obtained from the author upon reasonable request.

References

1. F. Zernike, "Beugungstheorie des Schneidenverfahrens und seiner verbesserten Form, der Phasenkontrastmethode," Physica **1**(7-12), 689–704 (1934).
2. F. Zernike, "Diffraction theory of the knife-edge test and its improved form, the phase-contrast method (English translation of the original publication in the German language," J. Micro/Nanolith. MEMS MOEMS **1**(2), 87–94 (2002).
3. W. T. Welford, "Length measurement at the optical resolution limit by scanning microscopy," In P. Mollet, editor, *Optics in Metrology*, 85–91. Pergamon Press, New York (U.S.A.), (1960).
4. M. Minsky, "Microscopy Apparatus," U.S. Patent 3,013,467 (1961).
5. W. T. Welford, "On the relationship between the modes of image formation in scanning microscopy and conventional microscopy," J. Microsc. **96**(1), 105–107 (1972).
6. D. Kermisch, "Principle of equivalence between scanning and conventional optical imaging systems," J. Opt. Soc. Am. **67**(10), 1357–1360 (1977).
7. T. Wilson and C. Sheppard, *Theory and practice of scanning optical microscopy*. Academic Press, Orlando, U.S.A. (1984), ISBN: 10.0127577602.
8. G. Bouwhuis and J. Braat, "Video disk player optics," Appl. Opt. **17**(13), 1993–2000 (1978).
9. J. Braat, "Optical video disks with undulating tracks," Appl. Opt. **17**(13), 2022–2028 (1978).
10. H. H. Hopkins, "Diffraction theory of laser read-out systems for optical video discs," J. Opt. Soc. Am. **69**(1), 4–24 (1979).
11. E. H. Linfoot, *Recent Advances in Optics*. Oxford at the Clarendon Press, London (U.K.), 1st edition (1955).
12. R. Gale Wilson, "Wavefront-error evaluation by mathematical analysis of experimental Foucault-test data," Appl. Opt. **14**(9), 2286–2297 (1975).
13. J. Villa, G. Rodríguez, I. de la Rosa, *et al.*, "Foucault test: shadowgram modeling from the physical theory for quantitative evaluations," J. Opt. Soc. Am. A **31**(12), 2719–2722 (2014).
14. D. Zagier, "The remarkable dilogarithm," J. Math. Phys. Sci. **22**, 131–145 (1988).
15. F. W. J. Olver, et al., *NIST Handbook of Mathematical Functions*, p. 359 and p. 610. Cambridge University Press, New York, N.Y. (2010).
16. B. M. Watrasiewicz, "Theoretical calculations of images of straight edges in partially coherent illumination," Optica Acta: International J. Opt. **12**(4), 391–400 (1965).
17. M. Born and E. Wolf, *Principles of Optics*, 7th expanded edition. Cambridge University Press, Cambridge, U.K. (1999).
18. J. W. Goodman, *Statistical Optics*. John Wiley & Sons, New York, U.S.A. (1985).
19. J. Braat and P. Török, *Imaging Optics*. Cambridge University Press, Cambridge, U.K. (2019).
20. P. H. van Cittert, "Die wahrscheinliche Schwingungsverteilung in einer von einer Lichtquelle direkt oder mittels einer Linse beleuchteten Ebene," Physica **1**(1-6), 201–210 (1934).
21. F. Zernike, "The concept of degree of coherence and its applications to optical problems," Physica **5**(8), 785–795 (1938).